Relativistic Laser Plasmas Generating Intense, Collimated Ion Beams

M. Roth[1], T.E. Cowan[2], J. C. Gauthier[3], J. Meyer-ter Vehn[4], M. Allen[5], P. Audebert[3], A. Blazevic[6], J. Fuchs[3], M. Geissel[6], M. Hegelich[7], S. Karsch[7], A. Pukhov[4], T. Schlegel[6]

[1]Gesellschaft für Schwerionenforschung mbH, Planckstr.1, 64291 Darmstadt, Germany
[2]General Atomics, P.O. Box 85608, San Diego, California 92186-5608
[3]Laboratoire pour l'Utilization des Laser Intense, Palaiseau, France
[4]Max-Planck-Institut für Quantenoptik, Garching, Germany
[5]University of California, Berkeley, USA
[6] Technische Universität Darmstadt, Germany
[7]Ludwigs-Maximilian Universität, München, Germany

The exploration of new regimes in plasma physics has been enabled recently by the advent of ultra-intense short pulse lasers [1] with intensities exceeding 10^{19} W/cm^2. The interaction of these laser beams with solid targets can produce gamma rays of tens of MeV, fast electrons of greater than 100 MeV and energetic ions with up to tens of MeV [2] in energy. The generation of fast protons from laser irradiated solid surfaces is attributed to electrostatic fields produced by hot electrons [3,4]. Relativistic electrons generated from the laser-plasma interaction, having an average temperature of several MeV, envelope the target foil and form an electron plasma sheath on the rear, non-irradiated surface. The electric field in the sheath can reach $>10^{12}$ V/m, which field-ionizes atoms on the surface and accelerates the ions very rapidly normal to the rear surface. Protons, having the largest charge-to-mass ratio, are preferentially accelerated in favor of heavier ions over a distance of a few microns, and up to tens of MeV. This forms a collimated beam with an approximately Maxwellian energy distribution at kT = 5-6 MeV. This acceleration mechanism makes these intense ion beams highly interesting for many applications, especially if one can collimate or focus the beam by shaping the target, as suggested by numerical calculations [5,6,7]. Therefore we carried out experiments to investigate in detail the influence of the target parameters on the ion beam production.

The experiments were performed with the 100 TW laser at Laboratoire pour l'Utilization des Laser Intense (LULI). Pulses of up to 30 J at 300 fs pulse duration at λ=1.05 μm were focused with an f/3 off-axis parabolic mirror onto free standing target foils at normal incidence, at intensity up to 5×10^{19} W/cm^2. The 1/e^2 focal spot radius measured in vacuum was about 5μm. Amplified spontaneous emission (ASE) occurred 2ns before the main pulse at a level of 10^{-7} of the main pulse energy and preformed a plasma.

A stack of radiochromic film (RCF) was positioned a few cm behind the target to measure the spatial beam profile. Two absolutely calibrated, permanent magnetic ion spectrometers were mounted at a distance of about 1m from the target covering a solid angle of 5x10^{-6} sr. The energy of the protons emitted normal to the target rear surface extended up to 25 MeV. The maximum energy of the protons dropped to about 13 MeV at an angle of 13°. The spectral shape of each proton energy distribution is generally continuous up to the cut-off energy, in agreement with the electrostatic sheath acceleration mechanism and as well as previously observed in experiments with the LLNL PETAWATT laser [2].

To investigate the influence of such target conditions on the creation of a collimated ion beam, we varied the target composition and structure of the rear surface.

We used thin (48 μm) targets of gold with either a flat or structured rear surface. The proton beam ejected from the rear surface is shown in Fig.1. The results showed a clear dependence of the spatial uniformity of the proton beam on the structure of the back surface. In contrast to the homogenous, collimated beam from the gold target, protons emitted from the structured gold rear surface showed filaments. To discriminate between conductivity and surface quality effects, we next used ~100 micron plastic and glass targets. The results of the glass and plastic targets were even more pronounced. While the flat surfaces of glass and plastic yielded a strong, but filamented proton beam, there were no protons detected above 1 MeV from the roughened targets. Using a Rasterscan-Electron-Microscope (REM) we examined the structure of the target surfaces (lower insets in Fig.1). Structuring the gold surface maintained a smooth surface with hills and valleys, visible as bright shadows on the lower right inset of Fig.1. The surface of the plastic and glass targets was largely destroyed by numerous cracks. The different behavior of the structured gold, glass and plastic targets can be understood within the context of the Target Normal Sheath Acceleration (TNSA) model [5]. When the material on the rear surface is exposed to the strong electric field generated by the electron plasma sheath, it is field ionized instantaneously.

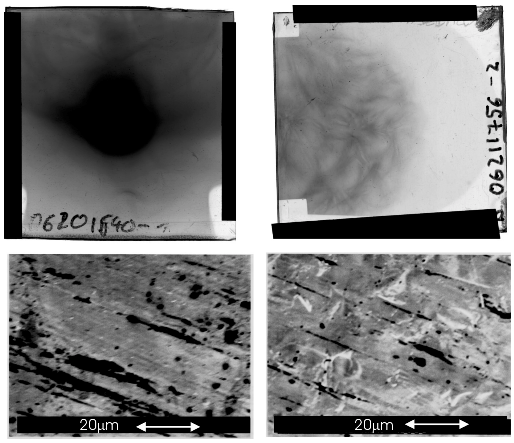

Fig. 1: Proton emission from smooth and roughened rear surfaces of a Au target. The roughened surface leads to the onset of filamentation. The REM images show the structure of the surface.

A shallow, wavelike surface, such as for the roughened gold targets, is expected to lead to a microlensing phenomenon, consistent with the observed filamentation or spatial modulation of the accelerated protons. Such effects have been calculated for the case of a single concave depression of the surface [5]. In the case of a destroyed surface, the cracks and defects on the plastic and glass create many sharp excursions, very different from the rather smooth undulating surface of the gold targets. The ion plasma created by the field is therefore extended over a much larger scale length normal to the (average) surface. We expect this to partially compensate the charge separation sheath, and therefore suppress the ion acceleration.

An important question to be addressed for any future application of laser-accelerated protons and ions is the possibility of tailoring the proton beam, either collimating or focusing it, by changing the geometry of the target surface. We first attempted to defocus the beam in one dimension by using a convex target. A 60 µm diameter Au wire as a target basically constituted such a one-dimensional defocusing lens, and we observed a line as shown in Fig. 2. Tilting the wire also changed the orientation of the line, which results from the radial, fan-shaped expansion of the protons normal to the wire.

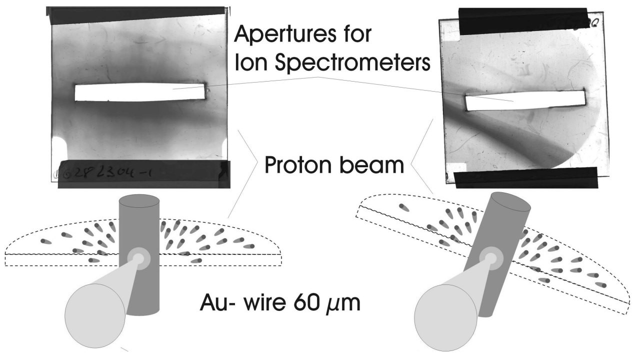

Fig. 2: Experimental setup and RCF images of experiments with 60 µm diameter gold wires. The convex rear surface constitutes a decollimating cylinder-lens. Accordingly the proton beam was formed into a line.

We then attempted to focus the protons by modifying the curvature of the target foil. Focusing of laser generated protons is essential for applications like ion-induced material damage research, proton fast ignition [8], proton radiography, and the use as next generation ion sources. Due to the gaussian-like shape of the hot electron debye sheath that causes the acceleration, there is an energy dependent angle of divergence that has to be compensated to focus the ions in the energy range of interest. Thus the effective focal length of a curved target rear surface is longer and dependent of the proton energy.

The curvature of the target surface used in these experiments was changed from a flat target to concave shaped targets with radii of curvature between 10 and 2.5 mm.

Fig.3 shows the experimental setup and the corresponding RCF images for a flat target and a target having a 2.5 mm radius of curvature. The RCF detector was mounted 9 mm behind the laser irradiated foil and protected from plasma blowoff by 10 µm of aluminum and 100 µm of titanium.

The respective ion energy in the layers of RCF corresponds to 5 MeV for the first layer and 7.5 MeV for the second. The results show a strong reduction in the divergence of the central core of the proton beam representing ballistic collimating of laser produced proton beams. For most of the future applications of laser generated ion beams the beam quality is the most important characteristic. As is apparent from the radiochromic film data, the angular divergence of the proton jet is rather well defined and decreases with increasing proton energy. This suggests that protons or other light ions accelerated by this mechanism may have a usefully small emittance in the sense of an actual ion beam.

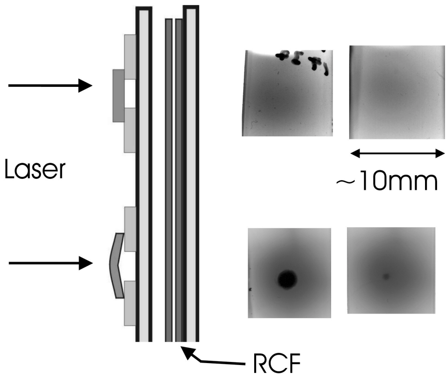

Fig.3: Focusing of laser generated proton beams. left: experimental setup. The RCF detector is shielded by 10 µm of aluminum and 100 µm of titanium. right: images of successive layers in RCF for a flat target and a target with 2.5 mm radius of curvature

To estimate our emittance, we used penumbral imaging of edges at different distances from the target with the magnetic spectrometers, to directly measure the core emittance of the proton beam. This technique is related to the conventional slit-emittance measurements made with apertures and screens at conventional accelerators. We determine the normalized emittance of protons from flat gold foils to be ~0.2 π mm-mrad, and a factor of at least two smaller than the resolution limited measurements we performed on the PETAWATT.

We have presented a detailed investigation of the target conditions on the proton and ion beam production from intense laser solid interactions. The observed strong dependence on the rear surface conditions is in agreement with the target normal sheath acceleration mechanism. The target conductivity appears to have a major influence on the quality of the ion beam, and the quality of the surface finish of the target is very important for maintaining a high gradient sheath and a laminar beam. It has been shown that tailoring the ion beam (yield, shape, homogeneity) by means of target shape and composition is possible, and we present first observations of laser-accelerated ion beam focusing.

The authors would like to thank the GSI target laboratory for the help designing the targets and for the REM measurements. This work was supported by the EU "Large Scale Facility Access Program"

References

1 M. Perry and G. Mourou, Science **264**, 917 (1994)

2 R.A. Snavely, et at., Phys. Rev. Lett. **14**, Vol 85, 2945 (2000)

3 S.J. Gitomer, Phys. Fluids **29**, 2679 (1986)

4 Y. Kishimoto, et al., Phys. Fluids **26**, 2308 (1983)

5 S.C. Wilks, et al., Phys. Plasmas, Vol. 8, 542 (2001)

6 H. Ruhl, et al., Plasma Physics Reports, in press, (2001)

7 A. Pukhov, accepted for publ. In Phys. Rev. Lett. (2001)

8 M. Roth, et al., Phys. Rev. Lett. **3**, Vol. 86, 436 (2001)

Spectroscopy of laser-generated ions and neutrons

S. Karsch[1,2], M. Hegelich[1,2], G. Pretzler[1,2], M. Roth[3], M. Geissel[3], A. Blaszevic[3], T. Schlegel[3], T. Cowan[4], M. Allen[4], P. Audebert[5], J. Fuchs[5], J.C. Gauthier[5], D. Habs[1] K.J. Witte[2], A. Pukhov[2], J. Meyer-ter-Vehn[2]
[1]LMU München, [2]MPQ Garching, [3]GSI Darmstadt, [4]General Atomics San Diego, [5]LULI Palaiseau

In recent laser plasma experiments, an intense and collimated beam of highly energetic protons was found to be emitted from the rear side of foil targets [1, 2, 3]. For example, using the Petawatt laser in Livermore, up to several percent of the laser energy was transferred into 2×10^{13} protons of energies $> 10\,\mathrm{MeV}$, with maximum energies above 58 MeV [4]. This effect is explained by an ultra-strong space charge field due to a relativistic electron cloud created by the laser pulse and located the backside of the target (TNSA mechanism [5]).

In previous experiments protons from surface contamination were found to be the dominant species to be accelerated independent of the target material.

In this experiment we tried to accelerate other ions as well by removing the contaminating layer. This was done embedded in a large experimental campaign at the 100-TW single shot laser at the Laboratoire pour l'Utilisation des Lasers Intenses (LULI) in Paris. The setup of our special experiment is shown in Fig. 1. Two Thomson parabola spectrometers distribute ions of one charge-to-mass ratio (q/m) on a parabolic trace according to their energy in the detector plane. CR39 nuclear track detectors recorded the traces.

We used 50μm aluminum targets with a rear-side 1μm carbon layer. Resistive heating led to a strong reduction of protons and an enhancement of carbon ions as obvious from Fig. 2. For quantitative analysis, single ion tracks on the CR39 films were counted by a scanning optical microscope [6]. First results suggest that C^4+ ions are dominantly accelerated with higher temperature and maximum energy than expected from linear interpolation. The full evaluation is under way and is expected to yield rich information on the dynamics of the ion acceleration mechanism.

In another experiment, targets with an amorphous CD-layer on the backside were used to produce a beam of accelerated deuterons. A CD_2 catcher target was positioned in this beam and $\sim 3 \times 10^7$ neutrons were generated, mainly by deuterium fusion.

At the MPQ ATLAS-10 laser facility, an adaptive optics system has been installed which consists of two deformable mirrors, wavefront and beam-profile diagnostics,

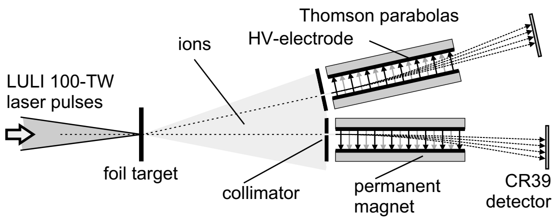

Figure 1: Setup for accelerating and diagnosing fast ions from the rear side of solid foils. Two Thomson parabolas were used at angles of 0° and 13° to the target normal.

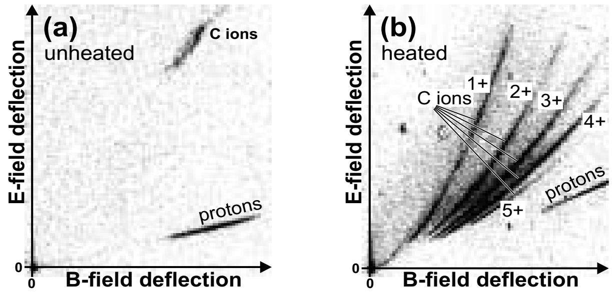

Figure 2: Thomson parabola spectra of laser accelerated ions. **(a)** Unheated target of $50\,\mu$m Al with a 1-μm layer of carbon at the rear surface. **(b)** Same target, but resistively heated for removing contaminating layers from the surface. The electric field in the Thomson parabola was different for the two shots.

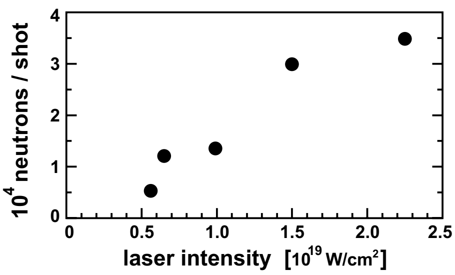

Figure 3: Dependence of the fusion neutron yield on laser intensity with solid CD_2 targets.

and automatic closed-loop alignment. The modifications now allow for reproducible high-intensity experiments up to $I > 2 \times 10^{19}$ W/cm^2. In ongoing fusion neutron generation experiments with solid CD_2-targets, a clear dependence of neutron yield on laser intensity has been found (Fig. 3). TOF spectroscopy of these neutrons allows to deduce the directional characteristics of the deuterons accelerated in the laser plasma, and a few different regimes were identified, with different angular deuteron distribution and probably with different acceleration mechanisms. (sup. by DFG Ha 1101/7-1, GSI F/E LM/HABP and EU Large Scale Facility Access Program)

References

[1] S.P. Hatchett et al., Phys. Plasmas **7**, 2076 (2000).
[2] E.L. Clark et al., Phys. Rev. Lett. **84**, 670 (2000).
[3] A. Maksimchuk et al., Phys. Rev. Lett. **84**, 4108 (2000).
[4] R.A. Snavely et al., Phys. Rev. Lett. **85**, 2945 (2000).
[5] S.C. Wilks et al., Phys. Plasmas **8**, 542 (2001).
[6] W. Rusch et al., Nucl. Tracks Radiat. Meas. 19, 261 266 (1991).

Characterization of Laser Heated Targets for UNILAC Beams

M. Geißel[1], E. Brambrink[1], A.Ya. Faenov[3], D.H.H. Hoffmann[1], T. Pikuz[3], P. Pirzadeh,[2], F.B. Rosmej[1], O. Rosmej[2], M. Roth[2], W. Seelig[1], J. Wieser[2]
[1]*TU Darmstadt*, [2]*GSI Darmstadt*, [3] *VNIIFTRI Mendeleevo, Russia*

An enhanced energy loss of heavy ions in laser produced plasmas compared with cold gas targets has been observed and studied at GSI for several years [1]. A thorough spectroscopic investigation of the properties of these plasmas was essential and first experiments have been carried out during the last two years [2]. The use of CF_2 targets instead of carbon enabled the application of spherically bent mica crystal spectrometers, which provide spatial and high spectral resolution [3], but an additional measurement of energy losses for carbon and CF_2 was pending to compare the behavior of the two materials.

Previous measurements used foils of 2 μm thickness or less. As CF_2 is available with a minimum thickness of 5 μm only, comparable shots with carbon and CF_2 could only be performed after an upgrade of the nhelix laser, which was completed during the year 2000. Table 1 shows the current performance of the upgraded laser.

Table 1: Data of the upgraded nhelix laser system

front end	Continuum Powerlite 8000 200 mJ @ 10 Hz
pulse width	12 ns
wavelength	1064 nm
number of amplifiers	5
number of spatial filters	4
energy	50 J
repetition rate	1-2 shots/hour
I_{max}	10^{12} W/cm^2

The comparison of CF_2 targets with 5 μm thickness and carbon targets with 1 mg/cm^2 ($\approx$ 4.5 μm) showed an almost identical values of carbon and CF_2. Although the measurements have an error level of about 10% both temporal evolution and signal amplitude show the same behaviour (Fig. 1).

The X-ray spectra show a high abundance of He-like and H-like Ions. While the H-like ions are concentrated in the hot region of interaction, the He-like ions can be observed throughout the jet-like expanding plasma [2]. The simultaneous observation of the X-ray emission from both front and rear surface by two seperate spectrometers enabled a further distinction of the homogeneity of the target plasma. It was shown, that similar properties are generated on both sides of the plasma (Fig. 2).

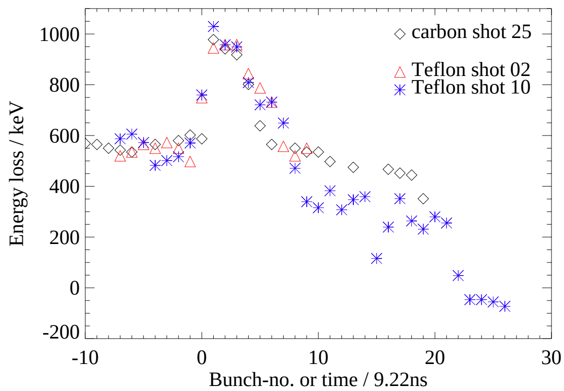

Figure 1: Comparison of different shots with carbon and CF_2 (Teflon) foil targets.

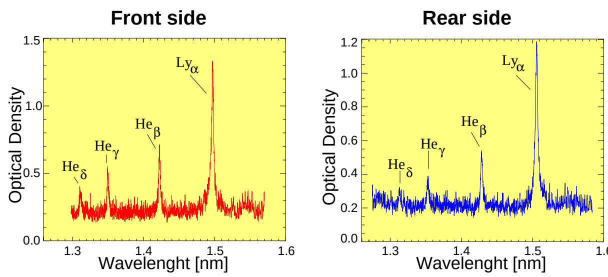

Figure 2: The comparison of X-ray spectra achieved on the front and rear surface shows similar conditions throughout the target.

References

[1] M. Roth, C. Stöckl, W. Süß, O. Iwase, D.O. Gericke, R. Bock, D.H.H. Hoffmann, M. Geißel, W. Seelig; Energy loss of heavy ions in laser-produced plasmas, Europhys. Lett., **50** (1), pp. 28–34 (2000)

[2] M. Geißel, R. Bock, A.Ya. Faenov, D.H.H. Hoffmann, T. Pikuz, P. Pirzadeh, F.B. Rosmej O. Rosmej, M. Roth; W. Süß, W. Seelig; GSI Scientific Report 1999, GSI-2000-1, p. 136

[3] I. Yu. Skobelev, A. Ya. Faenov, B. A. Bryunetkin, V. M. Dyakin, T. A. Pikuz, S. A. Pikuz, T. A. Shelkovenko, V. M. Romanova, A. R. Mingaleev; JETP **81**, 692ff (1995)

This work is supported by the BMBF of the Federal Republic of Germany, INTAS and WTZ

Advanced X-ray Diagnostics for Large Scale Dense Plasmas

F.B. Rosmej[1], D.H.H. Hoffmann[2,3], W. Süß[2,3], M. Geißel[2,3], A.Ya. Faenov[4], T.A. Pikuz[4]
[1]Université de Provence, Marseille, France, [2]GSI-Darmstadt, Germany
[3]TU-Darmstadt, Institut für Kernphysik, Germany, [4]VNIIFTRI MCISDC, Mendeleevo, Russia

Future GSI-experiments with intense heavy ion beams and the kilo-joule PHELIX-laser necessarily deal with large scale dense plasma objects. These plasmas might be either created by lasers to serve as a target for advanced studies of heavy ion beams interacting with matter or as intense back-lighter sources or may be created by intense heavy ion beams for, e.g., studies of strongly coupled plasmas.

The key issue and the request in common for the success of these experiments is a detailed characterization of large scale dense plasmas. Standard methods obviously fail due to the large optical thickness even for x-ray transitions. We therefore have undertaken an extended research program on this issue.

The novel aspect in this research is to base plasma diagnostic methods on forbidden line transitions with low transition probability A. This circumvents photo-absorption because the line center optical thickness τ_0 is proportional to A:

$$\tau_{0,ij} = \frac{1}{4}\lambda_{ji}^2 \frac{g_j}{g_i} A_{ji}\, n_i \left\{1-\frac{g_i n_j}{g_j n_i}\right\} \varphi_{ij}\left(\omega=\omega_{ji}\right) L_{eff}\,.$$

This approach, however, is highly non-trivial because transitions with low radiative decay values A are, first, difficult to observe and, second, they are highly dependent on density variations (because in dense plasmas collisional rates easily approach the radiative decay rate even for highly charged ions) and this denies their diagnostic use.

Despite these obstacles we have successfully developed a new concept for large scale dense plasma diagnostics introducing intercombination and two-electron transitions from autoionizing states as diagnostic and as reference lines [1,2]. We also performed atomic structure calculations to establish the required data [1].

.

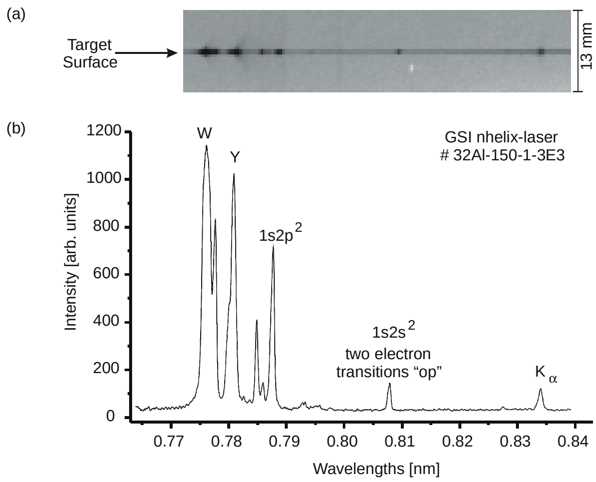

Figure 1: X-ray image of Al and spectrum near the target surface. Two-electron transitions have large intensity.

T

energies between 17 – 60 Joules, varying spot sizes from about 200 μm until 2 mm and laser pulse duration of 15 ns. Space resolved high resolution Argon K-shell X-ray radiation near $\lambda =$ 0.8 nm has been obtained with spherically bent mica crystals [3] and Kodak DEF X-ray film in the 2nd reflection order. X-ray images were digitized with a 10.000 dpi EUROCORE drum scanner. Spectra have been corrected for filter transmission, crystal reflectivity, film response and non-linear dispersion using SCALE.

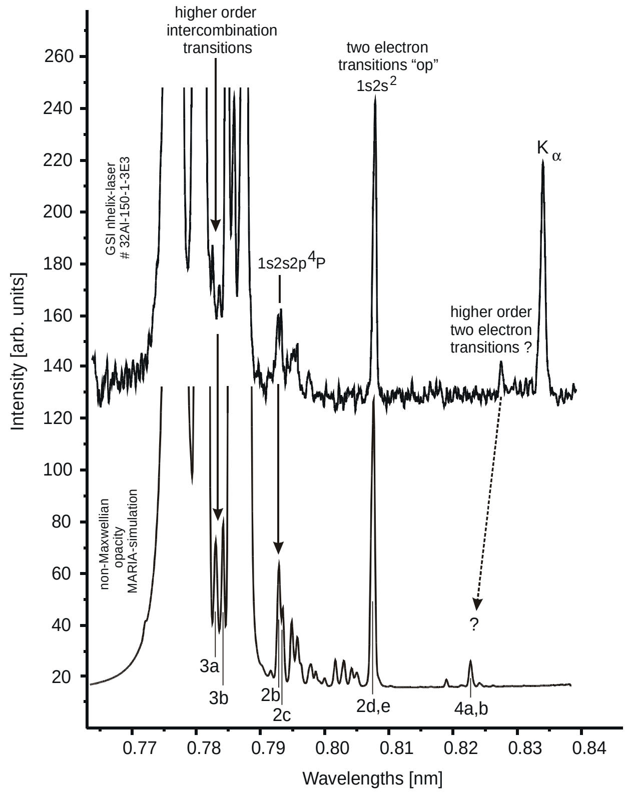

Figure 2: Large scale dense plasma diagnostic based on forbidden satellite transitions. Two-electron transitions serve as reference lines. Excellent agreement between the simulations and the experiment is obtained.

Figure 1 shows the plasma image and the corresponding spectrum near the target surface. Figure 2a demonstrates the intense observation of the requested forbidden satellite transitions. Fig. 2b shows the non-Maxwellian simulation which compares well with the experiment. The excellent agreement demonstrates the success of the present approach for the complicated case of large scale dense and non-Mawellian plasmas. The developed methods are therefore of general use and may readily be applied to PHELIX plasmas.

References

[1] F.B. Rosmej et al., Phys. Rev. A **63**, p032716 (2001).

[2] F.B. Rosmej et al., JQSRT, in print.

[3] I.Yu. Skobelev et al., JETP **81**, 692 (1985).

Projectile Spectroscopy: Space Resolved Registration of Projectile X-Rays Inside Matter

O.N. Rosmej[1], F.B. Rosmej[2], J. Wieser[1,3], M. Geißel[1,3], E. Brambrink[1,3], C. Niemann[1,3], A. Blazevic[1,3], K. Penache[1], D. Penache[1], J. Jacoby[1], E. Dewald[1], K. Weyrich[1], D.H.H. Hoffmann[1,3], A. Golubev[4], A. Borisenko[4]

[1]GSI-Darmstadt, Germany, [2]Université de Provence, Marseille, France,
[3]TU-Darmstadt, Institut für Kernphysik, Germany, [4]ITEP, Moscow, Russia

We report about the first successful observation of highly charged projectile radiation inside extended solid and gaseous matter at GSI. These investigations are of extraordinary interest for the physics of heavy ion beams interacting with matter because the x-ray spectra contain the information of the effective projectile charge state inside matter.

5.9 MeV/u Ni^{7+} with I = 100 pnA are interacting with Ar gas (p = 600-800 mbar). Figure 1 shows the X-ray emission of the K-shell spectra near λ = 0.16 nm of the multi charged Ni ions recorded in the 10^{th} reflection order as well as the argon K_α transition in the 4^{th} reflection order of spherically bent mica crystals [1]. Spectra emitted from different distances clearly show a variation of the nickel charge states.

Similar type of experiments were conducted with 5.9 MeV/u Ar^{7+} projectiles with I = 100 pnA interacting with massive aerogel targets (SiO_2, ρ = 0.1 g/cm^{-3}, crystal lengths about 2 mm). The argon projectiles are stopped inside the crystal after about 1.3 mm. Space resolved high resolution Argon K-shell X-ray radiation near λ = 0.4 nm have been obtained in the 4^{th} reflection order.

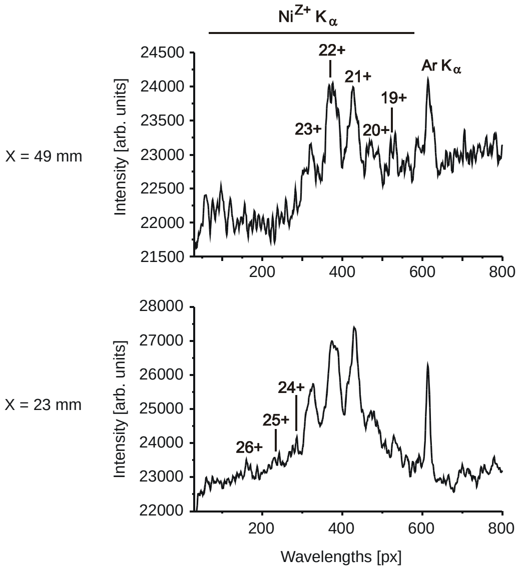

Figure 1: Space resolved X-ray spectra of Ni-projectiles

Figure 2 shows the characteristic K-shell emission of argon. The prominent spectral features are the H-like Ly_α lines 1s ^2S – 2p $^2P_{1/2,3/2}$, the He-like resonance line He_α = 1s2p $^1P_1$ – 1s^2 $^1S_0$ and Al K_α (used as a reference line). The high quality of the space resolved spectra is easily demonstrated by the resolved Ly_α doublet (Fig. 2b). The set of figures (a-c) demonstrates the simultaneously achieved space resolution, however, due to the partial destruction of the SiO_2-target the definite relation to the target locations is not possible. The spectral features on the red wings of the H- and He-like resonance lines are identified as dielectronic satellite transitions, 2l2l' – 1s2l" and 1s2l2l' – 1s^{2}2l" respectively. Detailed investigation of the satellite group formation shows asymmetries to the red wavelengths side for both, the He-like and Li-like (see, e.g., the arrow in Fig. 2a) transitions. The origin of these kind of asymmetries has recently been explored for dense hot plasmas [2], [3]: hot electrons preferentially increase the inner-shell excitation channel. In the present experiments, this channel is driven by the fast argon ions colliding with the target molecules T=SiO_2.

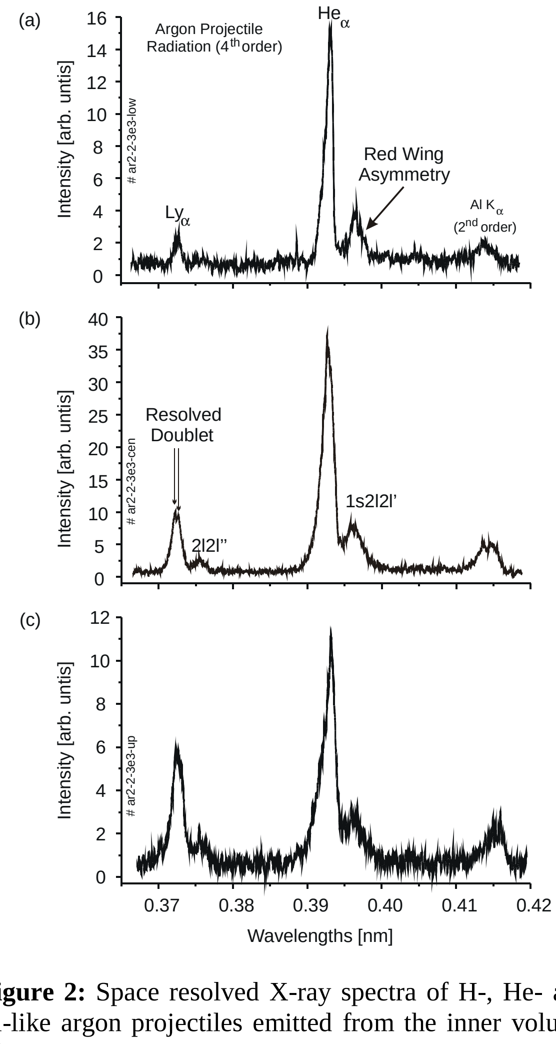

Figure 2: Space resolved X-ray spectra of H-, He- and Li-like argon projectiles emitted from the inner volume of an extended aerogel target

References

[1] I.Yu. Skobelev et al., JETP **81**, 692 (1985).

[2] O.N. Rosmej, F.B. Rosmej, 21st EPS Conference Proceedings on Controlled Fusion and Plasma Physics, Montpellier, France, Vol. III, p. 1292 (1994)

[3] F.B. Rosmej 1997, J. Phys. B Lett. **30**, L819.

This work is supported by the BMBF.

Optical Beam Diagnostics

J. Wieser[1], C. Constantin[2], E. Dewald[1], J. Jacoby[1], S. Udrea[2], D. Varentsov[2]
[1]*GSI-Darmstadt,* [2]*TU-Darmstadt*

The plasma-lens used at the HHT cave has been demonstrated to be a unique tool for shaping high energy ion beams into hollow beam spots [1] and achieving focal diameters, that are not accessible with regular magnets. However, electric currents on the order of 400kA within 9μs are necessary to achieve 10cm focal length. These currents, and the preionization pulses necessary for stable plasma formation, induce strong floating of the nearby ground-potentials, thus hindering low level electric measurements. In particular time resolved measurements of ion beam pulse intensities are strongly influenced by the plasma lens firing, as shown in Fig. 1.

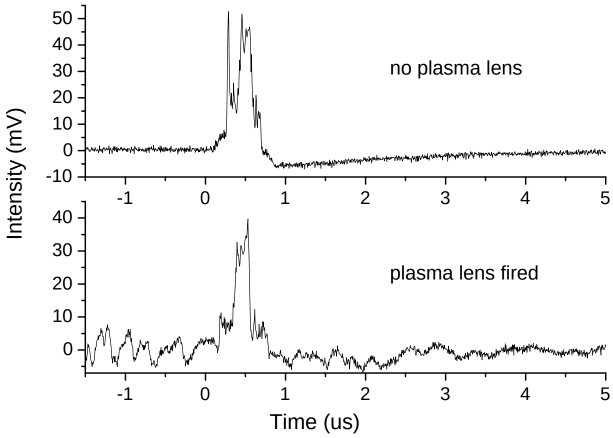

Figure 1: Fast current transformer signals of two different SIS pulses, without (upper) and with plasma lens fired (lower curve).

A first setup to circumvent this electric noise problem was installed, measuring the light emission from ion beam excited neon gas with a Si-PIN diode. Due to the optical measurement of the beam current, the system is rather insensitive to potential fluctuations and electric noise. A CF-100 double-cross was filled with 1bar neon, and the optical detector was placed in a distance of 0.5m. A D=2.5 neutral density filter had to be used for not overexposing the detector with an ion beam current of 2×10^9 Au particles per pulse. The signal to noise ratio increased by about one order of magnitude, without any additional means of shielding the signal lines (Fig.2).

Without plasma lens firing, the fast current transformer reflects well the temporal beam structure, except a negative overshoot after fast intensity drops. In order to simulate the optical signal, direct beam excitation of the light emitting species (neon 3p levels) is assumed, which then are supposed to decay within their natural lifetime of about 10ns. However, a 100ns decay time has to be used in order to coincide simulated and measured pulses, as shown in Fig. 3. This means that the 3p levels in neon, although no resonance transitions, are optically not thin and a linear response is not inherently given with the experimental conditions, used.

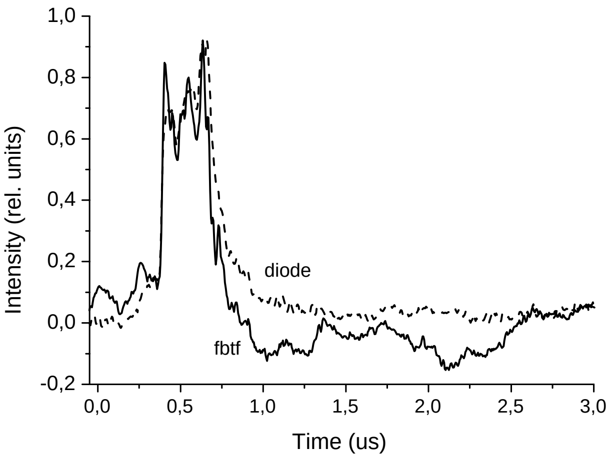

Figure 2: Comparison of the fast current transformer signal (fbtf, solid) and the optical signal (diode, dashed), with plasma lens fired. The entire pulse duration is 1μs.

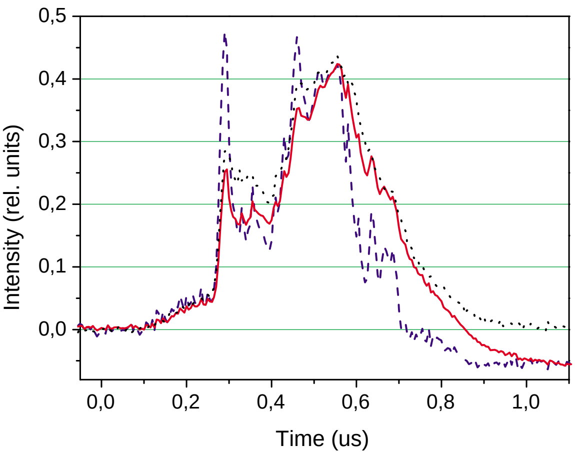

Figure 3: Without plasma lens fired, the signals of the fast beam transformer (dashed), the simulated optical signal (solid) and the measured diode signal (dotted) are given.

In a next set up, xenon will be used as a target gas, with a detector only sensitive to the molecular ion continuum radiation, not observing the 6p-6s transitions. In this way, a linear response over several orders of magnitude in ion beam intensities will be possible to be detected, with a linear response on a 5ns time scale, up to excitation densities of 10^{17}cm^{-3}.

work funded by BMBF

References

[1] U.Neuner et al., Phys. Rev. Lett. 85, 4518, (2000)

Diagnostics of Laser Initiated Plasma Channels for Ion Beam Transport

C. Niemann[1], D. Penache[2], A. Tauschwitz[2], F.B. Rosmej[2], S. Neff[1], R. Knobloch[1], D.M. Ponce[3] R. Presura[1], H. Wahl[1], S.S. Yu[3], W.M. Sharp[3], D.H.H. Hoffmann[2]
[1] *GSI Darmstadt,* [2] *TU-Darmstadt,* [3] *Lawrence Berkeley National Laboratory (USA)*

Laser initiated, free standing discharge channels offer many attractive advantages for the transport and focusing of intense ion beams [1, 2]. Discharge plasmas can neutralize both current and space charge of such beams, while the azimuthal magnetic field provides strong focusing all the way through the channel. Experiments at GSI have produced 50 cm long stable plasma channels with peak currents in excess of 40 kA in 2 to 20 mbar NH_3 gas fill. The discharges are initiated by a CO_2 laser pulse, fired into the chamber along the chamber axis. Absorption of the laser causes strong gas heating. Subsequent expansion and rarefaction of the gas prepare the right conditions for a stable, reproducible discharge, suitable for ion beam transport. First experiments to study the ion optical properties of such channels were already reported in [3, 4]. During the last year the channel stability was considerably improved by a new CO_2 laser with an option for wavelength tuning. The wavelength can be adjusted to the P(32) transition for peak absorption, matching the $\nu = 950\ cm^{-1}$ vibrational mode in NH_3 [5]. In this way a large fraction of the laser energy is absorbed as the beam passes through the 50 cm long gas filled chamber, down to pressures of a few mbar (figure 1).

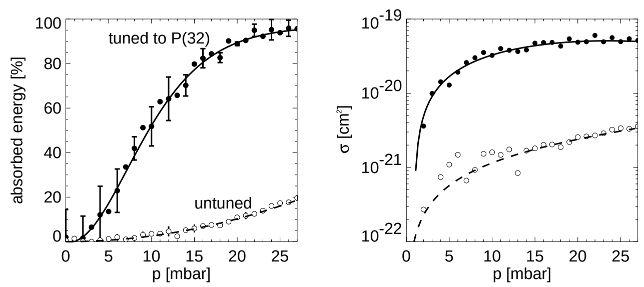

Figure 1: Improved laser gas heating due to laser wavelength tuning.

A set of plasma diagnostics was developed to gain a better understanding of the channel dynamics and the underlying physics. Schlieren measurements of neutral gas density gradients show a gas shock expanding radially with a velocity of a few $mm/\mu s$ while the discharge deposits its energy into the gas (figure 2). According to [6] this gas wall reduces the MHD instability growth rate and thus contributes to the stability of the channels. The plasma self emission was investigated by spectroscopy in the visible range. Electron densities around $10^{17} cm^{-3}$ can be estimated from Stark broadening of the observed hydrogen Balmer lines. Intensities of NII and NIII lines will be used to determine also the electron temperature. For more precise space resolved electron density measurements a Michelson imaging interferometer was set up. A pulsed Nd:YAG laser beam at 1064 and 532 nm with a diameter of several cm probes the plasma twice from a side and is then recombined with an undisturbed reference beam. The observed fringe shift (figure 2) yields the line integrated refractive index. The space resolved radial refractive index

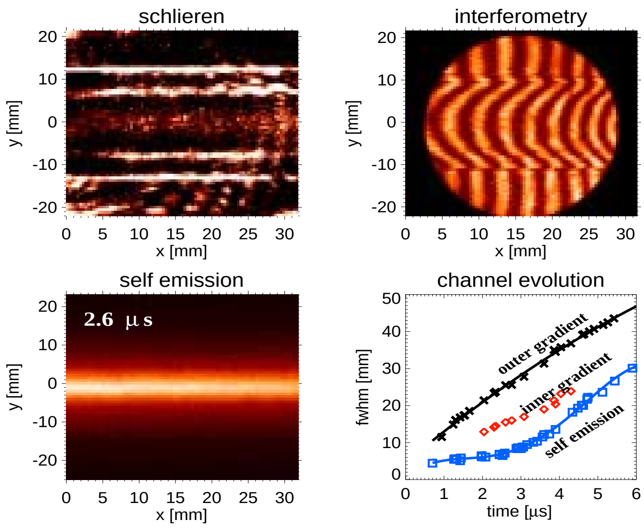

Figure 2: The channel as seen by different diagnostics.

profile follows from an Abel inversion. To distinguish between contributions from the electrons and the neutral gas to the refractive index the measurements were performed at both wavelength in subsequent discharges. A maximum fringe shift around 6 was observed at 1064 nm. A computer aided fringe counting method yields the fringeshift with a precision of around 0.2 fringes. Preliminary results are in agreement with spectroscopic density measurements.
These measurements in combindation with the ion optical investigations [7] will ultimately lead to a comprehensive understanding of the channel stability and dynamics. The results can then be used to engineer channels most suited for ion beam transport.

References

[1] A. Tauschwitz et al., Fus. Eng. Des. **32-33**, 493-502 (1996)

[2] S.S. Yu et al., Nucl. Instr. and Meth. A **415**, 174-181 (1998)

[3] D. Penache et al., GSI Report 1999(00), GSI-2000-1, p.125

[4] A. Tauschwitz et al., Proceedings: IFSA 1999, Elsevier, p. 521-526

[5] J.N. Olsen, J. Appl. Phys. **52**(5), 3279 (1981)

[6] W.M. Mannheimer et al., Phys. Fluids **16**, 7, 1126 (1973)

[7] A. Tauschwitz et al, this annual report

This work is supported by the BMBF

Ion Beam Transport in Discharge Channels: Interpretation of Experimental Results*

A. Tauschwitz, C. Niemann, D. Penache, S. Neff, R. Knobloch, H. Wahl, D.H.H. Hoffmann
GSI Darmstadt and TU Darmstadt

Discharge plasma channels are of interest for the current and space charge neutralized transport of intense ion beams for various applications. The channel transport in laser initiated discharges is currently studied at GSI [1]. In a series of experiments an uranium beam from the UNILAC with 11.4 MeV/u was transported through the 50 cm channel and was stopped in a fast scintillator behind the discharge. The picture at the left hand side of fig. 1 shows the force free drifting beamlets that are formed by a mask in front of the channel before the discharge is ignited. The mask consists of two perpendicular lines of 1-mm diameter holes with a distance of 2 mm between holes, forming a cross with the central hole missing. Three holes are drilled on each side, only two are visible, the last hole is clipped by the aperture in the cathode in front of the scintillator. An additional beamlet in the lower left sector serves to identify the orientation of the mask. The other seven pictures are taken at different times during the discharge with an exposure time of 100 ns. The exposure time, total

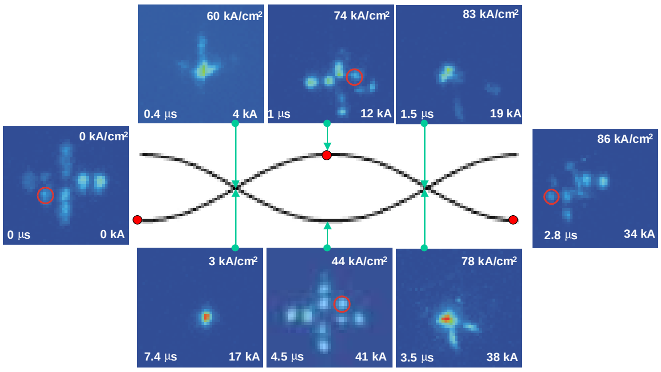

Figure 1: Image of the pepper-pot mask on the scintillator at different times during the first half wave of the current pulse

discharge current, and current density at exposure time are marked on the pictures. A representation of the betatron oscillation of the beamlets in the channel is shown in the center of fig. 1. The position of the asymmetric beamlet is marked by a dot. Arrows show at what phase of the oscillation the beamlets were intersected by the scintillator at the end of the discharge channel depending on the sinusoidal discharge current waveform. From the distortion of the image at 0.4 µs where a focal spot is expected, and at 1 µs where an inverted image is expected, it is obvious that the focusing field is nonlinear. At 1.5 µs the focusing is more linear and due to the expanding radius of the discharge channel the outermost beamlets become now visible as blurred spots below and right of the central spot. At a radius of 6 mm these beamlets were focused mainly in the decaying nonlinear magnetic field surrounding the discharge channel. At 2.8 µs the beamlets have performed a full betatron oscillation and the image of the mask is inverted twice. The outermost beamlets appear again as two blurred lines in the lower right sector of the cross. Although the total current is still increasing the current density and bending power of the channel is decreasing at 3.5 µs. The second focus is visible, the outermost beamlets show up more clearly now because the channel has expanded further and these beamlets were only for a short distance focused in the nonlinear field surrounding the channel. The peak current of 41 kA is reached at 4.5 µs, but due to the rapid expansion of the discharge channel the bending power is further decreasing so that the inverted image of the mask becomes visible again. At 7.4 µs the first focal spot appears again on the scintillator. By that time the channel has expanded to a diameter of more than 2 cm and the small size of the focus indicates a very linear field in the channel.

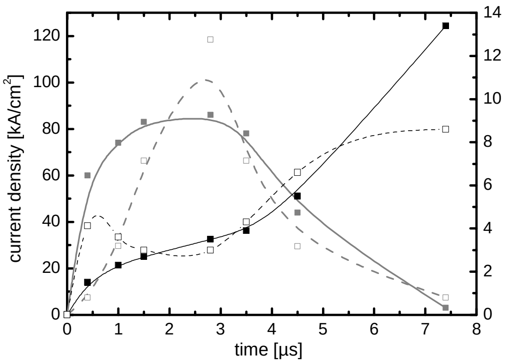

Figure 2: Development of current density and channel radius for a discharge in 17 mbar NH_3. Dashed lines are inferred from the beam transport assuming a homogeneous current distribution, solid lines from direct measurements.

An interpretation of the transport results is given in fig. 2. Measurements of the discharge current were evaluated together with framing pictures of the discharge channel to determine the discharge radius and the current density. For a first simple modelling the FWHM value of the light emission from the channel was assumed as the width of a homogeneous current distribution. The resulting radius and current density are plotted as solid lines in fig. 2.

$$J = \frac{2\pi\Re}{\mu_0}\left(\frac{kL}{L}\right)^2 \qquad (1)$$

Assuming again a homogeneous current flow in the discharge a current density J was determined according to equ. 1 from the phase of the beam betatron motion of the beamlets from fig. 1 with the beam rigidity $\Re$ and a phase kL of the betatron oscillation at the end of a channel with length L. For the first focal point, the inverted image, the second focus, and for the twice inverted image the phases of the oscillation are $\pi/2$, π, $3\pi/2$, and 2π respectively. The current density from equ. 1 and the resulting discharge radius are plotted in fig. 2 with dashed lines. Deviations during the first microsecond can be explained by the skin effect in the discharge, deviations at the end of the current half wave are probably due to the inverse skin effect [2].

References

[1] A. Tauschwitz et al. Proc. Int. Conf. on Inertial Fusion Sciences and Applications (IFSA), Bordeaux, 521 – 526 (1999)

[2] M.G. Haines, Proc. Phys. Soc. **74**, 576-586 (1959)

* work supported by BMBF

Electrical Conductivity Changes Induced by High Intensity Heavy Ion Beams in Metallic Targets

S. Udrea[1], E. Dewald[2], C. Constantin[1], D. Varentsov[1], J. Jacoby[2], U. Neuner[2], A. Tauschwitz[1], P. Spiller[2], D.H.H. Hoffmann[1,2]
TU-Darmstadt[1], GSI-Darmstadt[2]

The electrical conductivity of matter under extreme pressure and/or temperature conditions is of fundamental as well as practical interest [1]. The availability of high intensity heavy ion beams at GSI makes it possible to drive matter to extreme conditions, either through direct interaction or shock wave compression. As previously reported [2], we developed a method for measuring the mean electrical conductivity of plasmas created by direct interaction. During the last year this method was applied to obtain first experimental results on electrical conductivity changes induced by the interaction of high intensity heavy ion beams with solid (metallic) targets.

For the experiments Pb, Cu, Ag and Al were used as target materials. All the targets consisted of a 0.25mm diameter and 10mm long wire fixed on an insulating support and connected to the diagnostics device through a 50Ω coaxial cable. Measurements were done using two different positions of the target, namely, perpendicular to the focused ion beam due to an easier mechanical adjustment of the wire related to the beam, and along the focused ion beam which is demanding in terms of alignment but should give better measurement precision. During the different beamtimes ion beams with the following characteristics were used: ^{83}Kr, 300MeV/u, $1\div2\cdot10^{10}$ ions/bunch; ^{197}Au, 300MeV/u, $1\div2\cdot10^{9}$ ions/bunch; ^{18}O, 200MeV/u, $1\div2\cdot10^{10}$ ions/bunch; ^{40}Ar, 300MeV/u, $5\div8\cdot10^{10}$ ions/bunch.

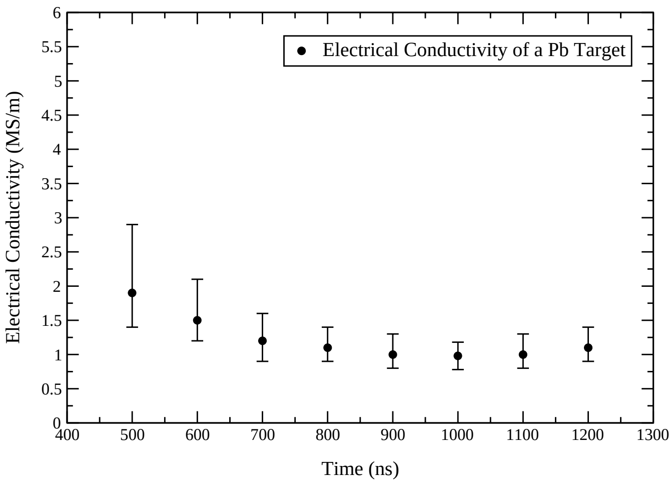

Figure 1: Mean electrical conductivity of a Pb target heated by a ^{18}O beam, with an intensity of $2\cdot10^{10}$ions/bunch, and focused to 0.7mm FWHM. The time is given with respect to the beginning of the irradiation.

The electrical signal obtained from the target is proportional to the changes of its resistance and thus to the changes in the mean electrical conductivity. Figure 1 shows the time evolution of the electrical conductivity of a Pb target irradiated by an ^{18}O beam.

The measurements show that at the end of the beam irradiation, the conductivity of the target corresponds to that of metals at temperatures of about 10^{-1}eV, and solid state density [3]. Due to the hydrodynamic expansion of the target, the conductivity drops in time, thus the electrical resistance grows. The rate at which this conductivity

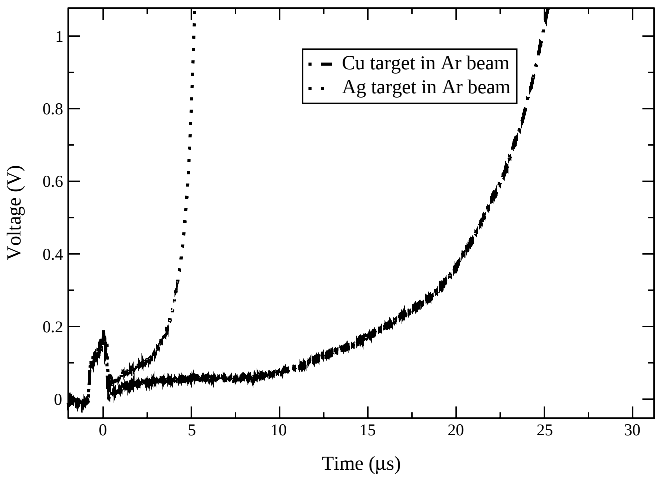

Figure 2: Electrical signals from Cu and Ag target heated by a ^{40}Ar beam, with an intensity of $7\cdot10^{10}$ions/bunch, and focused to 1.0mm FWHM. The beam bunch is visible arround t=0.

drop takes place depends strongly on the energy deposited in the target by the ion beam (i.e. on ion species and energy, beam intensity and focusing, and target material) and the thermodynamic properties of the target. This differences are shown in Figure 2.

Acknowledgements: The authors acknowledge the help of Dr. N.A. Tahir and A. Kozyreva in understanding the theoretical aspects of these experiments and the numerical simulations of the hydrodynamics of the target. This work is supported by the BMBF.

References

[1] G.W. Collins et al., Science 281 (1998) 1178
[2] S. Udrea et al., GSI Scientific Report 1999
[3] Gmelins Handbuch der Anorganischen Chemie, Verlag Chemie GmbH, 1972

Schlieren investigations on pressure waves induced by the heavy ion beams in solid targets

C. Constantin[1], E. Dewald[2], C. Niemann[2], S. Udrea[1], D. Varentsov[1], U.N. Funk[1], D.H.Hoffmann[1]
J. Jacoby[2], U. Neuner[2], P. Spiller[2], A. Tauschwitz[1]
TU-Darmstadt[1],*GSI-Darmstadt* [2]

The intense relativistic heavy ion beams generated in the heavy ion synchrotron (SIS) of GSI offer the possibility to study the matter under extreme conditions. This is a subject of many on-going experiments at HHT area of GSI, such as investigations on the hydrodynamical evolution and cold compression of the matter supressed to the high energies delivered by the ion beam. The adiabatical cold compression of solid state matter is relevant for equation of state (EOS) studies including phase transitions to metallic state [1]. In one of these experiments a $^{83}Kr^{36+}$ ion beam with $2 \cdot 10^{10}$ particles/pulse, 300 MeV/u energy and 700 ns pulse duration was stopped in a solid layered target which is described in the graphic below (fig.1).

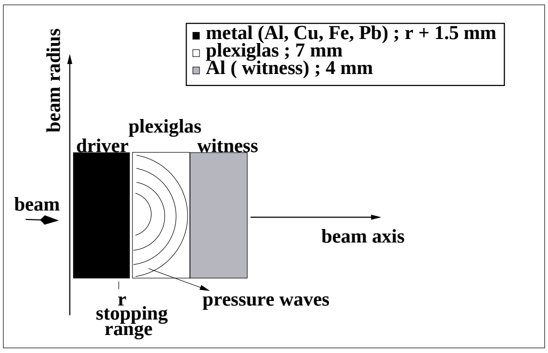

Figure 1: The target design: metal driver, 7 mm plexiglas window, 4 mm Al witness for observing the reflexions on interfaces between different materials.

After the beam is stopped in the driver pressure waves are launched and propagate in the plexiglas. To visualise and characterise them a schlieren technique was employed. Schlieren method is based on the bending of light rays when passing through refractive index gradients perpendicular to the optical path. The perturbances induced by the pressure waves in the target create regions of density gradients which will deflect some rays of the initially parallel laser beam towards the higher densities; these rays will no longer follow the parallel beam which is blocked by a beam stop put in the focus of the laser beam. They will pass near by and will be recorded on the detectors.The time resolved detection in this case was done by a streak camera working in a 10 μs streak time mode. The time resolution given by the streak slit width was of 180 ns and a very strict focusing on the target insured the space resolution. A framing camera was mounted together with the streak camera for two dimensional visualisation of the shock front. The 2D pictures so obtained showed a spherical wave expanding in time. From the streak pictures it was possible to determine the propagation velocity, which was found to be slightly higher than the speed of sound in plexiglas (2.6 km/s). The velocity and the consequently determined pressure values [2] depend on the heavy ion beam energy deposition in the driver material. For the Kr ion beam and all four materials this values are tabulated below (table 2).

species	driver	velocity [km/s]	pressure [Gpa]
$^{83}Kr^{36+}$	Al	2.82	0.26
	Fe	2.74	0.21
	Cu	2.70	0.16
	Pb	2.92	0.40

A typical behaviour for shock waves is to split whenever an interface between two materials with different acoustic impendences is encountered [3]. Due to this fact multiple pressure waves could be seen in the experimental pictures together with their reflections on the plexiglas boundaries (fig.2). Future experiments will consist in several optimizations regarding the target geometry and moddeling of the shock front, i.e. to obtain planar shock waves, much more effective also from the investigation point of view. As a result, also an increase in the compression factor (around 0.04 in the actual conditions) is expected. The experimental set-up will be oriented towards absolute measurements of three main parameters: velocities of the shock wave propagation, pressures behind the shock waves and densities in the sample material. These results would constitute reliable benchmarks for the theoretical simulations and EOS studies.

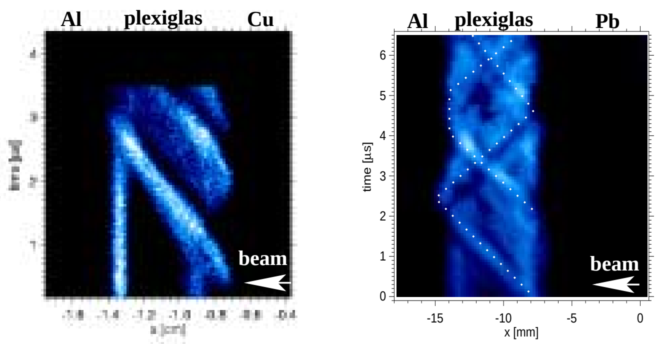

Figure 2: Experimental picture of a Pb-plexiglas-Al and Cu-plexiglas-Al target shooted with a Kr ion beam.

Acknowledgments: We thank BMBF for supporting this work.

References

[1] N.A. Tahir, D.H.H. Hoffmann et al.: Phys.Rev.E, vol.16, no.2 (2000) 1975-1980

[2] Bao-Ping Zhang, F. Mueller: High Temperatures-High Pressures, volume 16 (1984) 475-483

[3] K. Baumung, H.J. Bluhm et al.: Laser and Particle Beams, vol. 14, no.2 (1996) 181-209

Shadowgraphy measurements on the heavy ion beam interaction with solid targets

E. Dewald[1], C. Constantin[2], S. Udrea[2], D. Varentsov[2], D.H.H. Hoffmann[2,1], J. Jacoby[1], U. Neuner[2], A. Tauschwitz[2], J. Wieser[1], N.A. Tahir[2], A Kozyreva[2], U. Geißler[2], M. Roth[1], P. Spiller[1] and R. Bock[1]
[1]GSI Darmstadt, [2]TU-Darmstadt

At the HHT experimental area, strongly coupled plasmas are created by the interaction of the SIS heavy ion beams with solid targets. To obtain a high energy deposition in the target, the ion beam is focused by the plasma lens [1] to diameters smaller than 1 mm in the focus. The generated plasmas have densities close to the solid state density, volumes of several mm^3 and temperatures up to 1 eV. The characterization of the matter under such extreme temperatures and pressures is of relevance for equation of state (EOS) studies, in astrophysics for understanding the formation of heavy elements in supernovae, for designs of future heavy ion driven Inertial Fusion Experiments (IFE) and others.
A wide range of optical diagnostics, such as shadowgraphy, time resolved spectroscopy in visible and VUV ranges, and schlieren techniques were recently developed to study the target behavior at the interaction with the ion beam.
Up to now, metallic and cryogenic gas crystal targets [2] were used for the ion beam heating experiments, characterized by backlighting shadowgraphy and time resolved spectroscopy. For these experiments the backlighter was a high energy (250 J) Xe flashlamp and the target dynamics was detected with a fast multiframing camera, capable to acquire simultaneously eight frames with an exposure time above 10 ns.

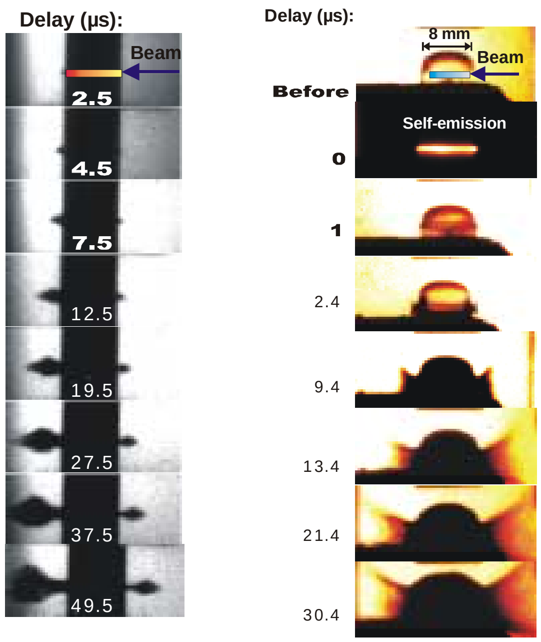

a *b*

Figure 1: Superrange target dynamics in beam-target interaction experiments for 1 μs beam duration (50-200 ns exposure):
(a) 6 mm thick Pb plate, Kr beam, 300 MeV/u, $N=10^{10}$ ions,
(b) 8 mm Ne crystal, U beam, 200 MeV/u, $N=10^9$ ions

Figure 1 shows typical hydrodynamics of targets larger than the ion beam range, for metallic plates and cryogenic gas crystals. Due to the non-uniform energy deposition, for the Pb plate (Fig. 1a) the matter expansion in the Bragg peak region is clearly more pronounced than in the direction opposite to the beam as it can be seen also in Figure 2. Moreover, due to a strong radial temperature decrease from the axis, the heated expanding matter has a droplet shape. For EOS studies the experiments are simulated by the BIG2 two-dimensional hydrodynamic code. According to the simulation, a maximum temperature of 0.3 eV is reached in the plate by ion beam heating. The matter expansion velocity is used to benchmark the simulation.

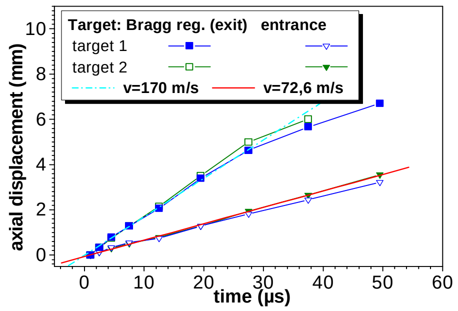

Figure 2: Axial matter expansion for the Pb plate (Fig. 1a)

Quite a different behavior was observed for the cryogenic gas targets, i.e. for most of the crystals there is a symmetric matter expansion even for targets thicker than the ion beam range (Fig.1b). This is mainly explained by the drilling effect of the beam which shifts the range during the beam pulse beyond the target thickness. This can be experimentally observed from the target self-emission and 1 μs after the beam (Fig 1b). For a specific energy deposition of 6.8 kJ/g, a maximum temperature of 0.48 eV is reached in the Bragg peak region according to the BIG 2 simulation. Furthermore, the Bragg peak in the crystals is less pronounced than in the metal plates which results in a more uniform energy deposition. A high expansion velocity (470 m/s) was observed in the first 5 μs, after which it decreases in 10 μs to a constant velocity of 140 m/s. For cryogenic crystals this behavior was already predicted in [3].
Another interesting feature is that the radial shockwave generated by the heated matter destroyes the crystal structure and consequently its transparence as it can be observed in Fig. 1b for the pictures taken 1, 2.4 and 9 μs after the beam.
Several experiments were performed using different ion beams, cryogenic crystals (H, D, Ne, Ar, Kr, Xe) and metallic plates.
The shadowgraphy measurements give an insight into the beam-target interaction and into the generated plasmas. Furthermore, the matter dynamics can be used to benchmark the simulation code as well as the used EOS data.
Acnowledgement: This work was supported by BMBF.

References

[1] M.Stetter et al., Fus. Eng. Des. 32-33(1996) 503
[2] U.N.Funk et al., Nucl. Inst. And Meth.A 415 (1998) 68
[3] M. Dornik, Ph.D. Thesis, TU Darmstadt, 1997

Necessity for Strong Bunch Compression for the SIS-200 Beam for FRS and Plasma Physic Experiments

N. A. Tahir[1], A. Kozyreva[1], D. H. H. Hoffmann[1,2], P. Spiller[2], A. Shutov[3]
[1]TU Darmstadt, [2]GSI Darmstadt, [3]ICPR Chernogolovka

GSI is planning to build a new synchrotron, SIS-200, that will have a magnetic rigidity of 200 Tm. It will be designed to accelerate 10^{12} uranium particles with energy ranging from 200 MeV/u to 1 GeV/u. The plasma physics experiments will require a lower energy of 200-400 MeV/u while the fragment separator (FRS) experiments would be carried out using 1 GeV/u.

The temporal profile of the beam is very important for these experiments. To demonstrate this we simulated hydrodynamic and thermodynamic response of a "sub-range" solid lead cylindrical target that is irradiated with the future SIS-beam with parameters given above. These simulations have been done using a two-dimensional computer code, BIG-2 [1]. The beam-target geometry is shown in Fig. 1.

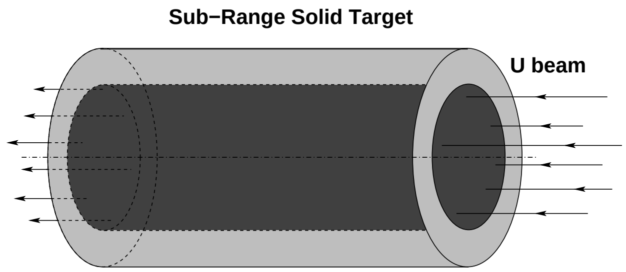

Figure 1: A "sub-range" lead target irradiated by 1 GeV/u uranium beam.

We considered two beam power profile configurations. First we assumed five identical parabolic bunches as showm in Fig.2. Each bunch is 140 ns long and every bunch contains 2×10^{11} particles. Bunch separation is also 140 ns so that the duration of the pulse is 1260 ns.

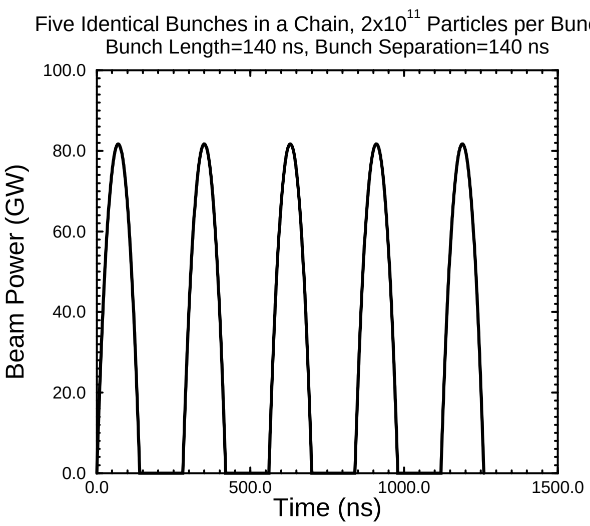

Figure 2: Beam Power vs Time.

In Fig. 3 we plot the energy of the ions escaping the target as a function of time along the axis for two values of the beam radius (FWHM), 0.5 mm and 1.0 mm respectively. It is seen that innitially, 75 % of the energy escapes the target. However at t = 140 ns, that is at the end of the first bunch, the fraction of the energy escaping the target increases considerably due to the hydrodynamic expansion of the target material caused by beam heating. The target continues to expand for the next 140 ns until the second bunch starts at t = 280 ns. Figure 3 shows that almost the total ion energy escapes the target. It is therefore clear that due to the target distortion caused by the first bunch, the ions that are delivered in the remainig four bunches pass through the target without interaction. Bulk of the beam energy is therefore wasted. In case of plasma physics experiments, such a reduction in beam-target coupling would lead to a strong reduction in temperature and pressure that could be achieved. For the FRS experiments, the production of fragments will decrease drastically. Also the fragment separator can accept only a few percent change in the energy of the escaping ions, otherwise most of the secondary beam will be lost.

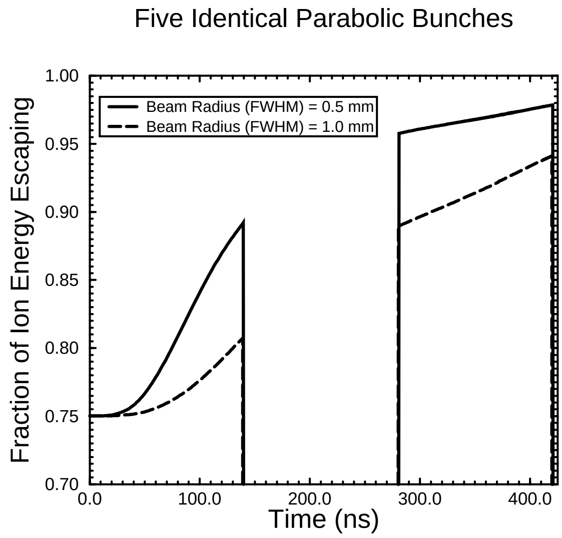

Figure 3: Energy of Ions Escaping the Target vs Time.

These diffuculties may be overcome by using a highly compressed single bunch with a length = 50 ns. For further details see Reference [2].

References

[1] V. E. Fortov et al., Nucl. Sci. Eng. 123 (1996) 169.
[2] N. A. Tahir, A. Kozyreva, P. Spiller, D. H. H. Hoffmann and A. Shutov, Phys. Rev. E (2001) 036407.

Supported by the German ministry for education and science (BMBF)

Simulation of Hydrogen Metallization Experiment Using the SIS-200

N. A. Tahir[1], A. Kozyreva[1], D. H. H. Hoffmann[1,2], A. Shutov[3], J. A. Maruhn[4], P. Spiller[2], U. Neuner[2], A. Tauschwitz[2], J. Jacoby[2], M. Roth[2], R. Bock[2], H. Juranek[5], R. Redmer[5]
[1]TU Darmstadt, [2]GSI Darmstadt, [3]ICPR Chernogolovka, [4]Universität Frankfurt, [5]Universität Rostock

This contribution presents two-dimensional hydrodynamic simulations of a cylindrical multi-layered target that contains a layer of frozen hydrogen and is irradiated by a uranium beam. These simulations have been done using the BIG-2 [1] computer code. The beam-target arrangement is shown in Fig. 1. The target is 3.0 mm long and the radius of the hydrogen layer is 0.5 mm whereas the outer target radius is 3.0 mm. The right face of the cylinder is irradiated with the SIS-200 beam. The beam consists of 10^{12} particles of U 400 MeV/u and the pulse length = 50 ns. The beam spot has an annular shape (ring shape). The inner radius of the focal spot ring is also 0.5 mm while the outer radius is 2.0 mm. This avoids direct heating of the hydrogen region. The range of 400 MeV/u uranium ions in solid cold lead is 4.25 mm. The energy deposition is therefore approximately uniform in the lead shell because the Bragg peak lies outside the target.

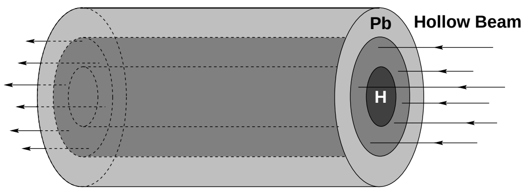

Figure 1: A Multi-Layered Cylindrical Target Driven by 400 MeV/u Uranium Beam

Figure 2 shows the density vs radius at L = 1.5 mm (middle of the cylinder) in the hydrogen region at different times during the implosion. It is seen that at t = 100 ns, a shock has entered into the hydrogen region and the shock front is at r = 150 μm. Moreover the hydrogen-lead boundary has moved from an initial position of 500 μm to about 350 μm. The shock converges at the cylinder axis at t = 115 ns and a return shock developes that is seen moving outwards at t = 120 ns. The return shock is again reflected at the hydrogen-lead boundary that continues to move inwards slowly. As a result of this multiple shock reflection and slow adiabatic compression, the hydrogen layer is compressed to physical conditions predicted for hydrogen metallization. These include a density of about 1 g/cm^3, a pressure of above 3 Mbar and a temperature of a few 0.1 eV. The SESAME equation-of-state data is used for hydrogen.

In Fig. 3 we plot the density, pressure and temperature vs radius in the hydrogen region at L = 1.5 mm at t = 170 ns. It is seen that the density is about 1 g/cm^3, the average temperature is about 0.2 eV while the pressure is above 5 Mbar. These conditions exist between t = 160 ns - 200ns which provides with enough time for experimental investigations. For details see Refs. [2,3].

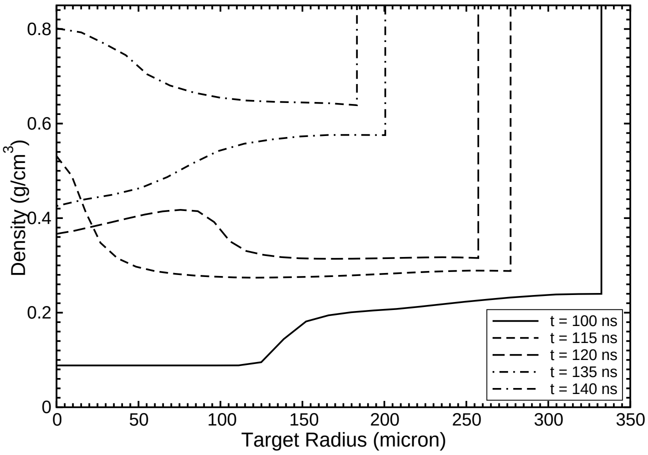

Figure 2: Density vs Target Radius at L = 1.5 mm

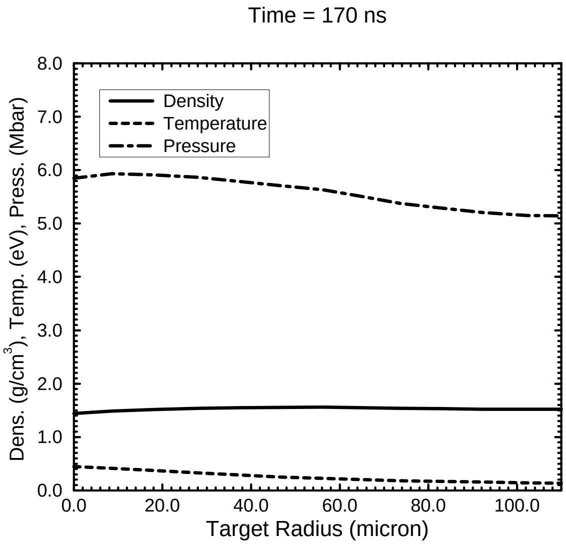

Figure 3: Density, Temperature and Pressure vs Target Radius at $L = 1.5\,\mathrm{mm}$ and at $t = 170\,\mathrm{ns}$.

References

[1] V. E. Fortov et al., Nucl. Sci. Eng. 123 (1996) 169.
[2] N. A. Tahir, D. H. H. Hoffmann, A. Kozyreva, A. Tauschwitz, A. Shutov, J. A. Maruhn, P.Spiller, U. Neuner, J.Jacoby, M.Roth,R. Bock, H. Juranek and R. Redmer, Phys. Rev. E 63 (2001) 016402.
[3] N. A. Tahir, D. H. H. Hoffmann, A. Kozyreva, A. Tauschwitz, A. Shutov, J. A. Maruhn, P.Spiller, U. Neuner, J.Jacoby, M.Roth,R. Bock, H. Juranek and R. Redmer, Contrbu. Plasma Phys. (2001) In Print.

Supported by the German ministry for education and science (BMBF)

Calculation of the Current Density Distribution in a Plasma Lens to Produce Ring-like Ion Beam Profiles

S. Hakuli, U. Neuner
GSI Darmstadt and Institut für Kernphysik, TU Darmstadt

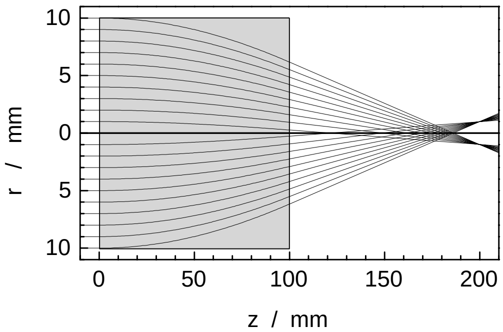

Figure 1: Schematic of focusing a 10 mm radius parallel ion beam into a 1 mm radius ring with a 100 mm long plasma lens with a negative radial gradient of the current density and a 100 mm long drift length.

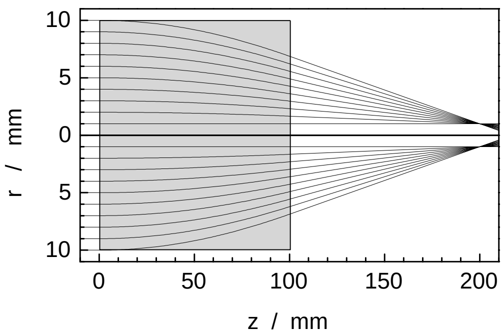

Figure 2: Same as Fig. 1 with a positive radial gradient of the current density.

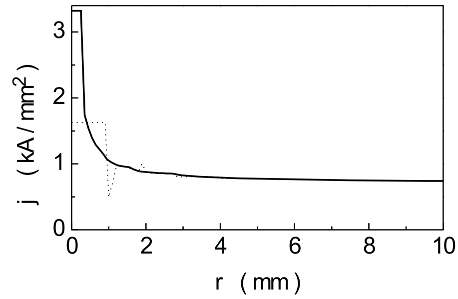

Figure 3: Current density distribution in the pinch mode.

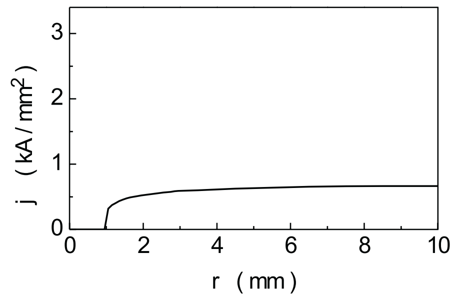

Figure 4: Current density distribution in the skin mode.

A good understanding of the shaping of intense ion beams into hollow cylindrical form [1] was achieved by interpreting the experimental data [2] with numerical calculations.

The ion beam is shaped in a plasma lens, where an axially directed current produces an azimuthally directed magnetic field. In this field the ion trajectories of an initially parallel beam are bent towards the axis. This allows for the two focusing schemes plotted in Figs. 1 and 2, where all ion trajectories between 1 and 10 mm initial radius converge into a ring in the focal plane 100 mm after they exit from the plasma lens.

We simulated this focusing for a zero emittance beam in paraxial approximation. Since ions pass through radial regions of different focusing strength inside the plasma lens, the calculations were performed as follows: We divided the plasma lens into 100 thin slices, in which the radial variation of the trajectory is so small, that the focal strength can be approximated to be constant. The shape of the trajectories results from a calculation of the Lorentz force inside the plasma lens' slices. The radial current density distribution is discretized into shells of constant values. Increasing in radius one-dimensional nonlinear optimizations yield these values for the two focusing modes as mentioned above.

The solid curve in Fig. 3 shows the calculated current density in the plasma lens as a function of radius, that leads to focusing into a ring as shown in Fig. 1. Such a negative radial gradient can be realized in a pinch-like discharge. The dotted curve is also a valid solution for this focusing, however it seems unlikely to be realized in any known discharge. The current density in Fig. 4 corresponds to the focusing mode shown in Fig. 2. Positive radial gradients like this can be realized in skin effect dominated discharges.

With these results we now can experimentally optimize the plasma lens to produce ideal hollow cylinder shaped beams. They are required by the future experiments [3, 4, 5, 6].

References

[1] U. Neuner *et al.*, Phys. Ref. Lett. **85**, 4518 (2000).

[2] U. Neuner *et al.*, GSI-2000-1, 127 (2000) and GSI-2000-2, 3 (2000).

[3] D. A. Callahan-Miller and M. Tabak, Nucl. Fusion **39**, 1547 (1999).

[4] D. A. Callahan-Miller and M. Tabak, Phys. Plasmas **7**, 2083 (2000).

[5] N. A. Tahir *et al.*, Phys. Rev. E **62**, 1224 (2000).

[6] N. A. Tahir *et al.*, Phys. Rev. E **63**, 016402 (2001).